University Library



A gateway to Melbourne's research publications

Minerva Access is the Institutional Repository of The University of Melbourne

Author/s:
Harris, AR

Title:
Understanding charge transfer on the clinically used conical Utah electrode array: Charge storage capacity, electrochemical impedance spectroscopy and effective electrode area

Date:
2021-04-01

Citation:
Harris, A. R. (2021). Understanding charge transfer on the clinically used conical Utah electrode array: Charge storage capacity, electrochemical impedance spectroscopy and effective electrode area. Journal of Neural Engineering, 18 (2), https://doi.org/10.1088/1741-2552/abd897.

Persistent Link:
https://hdl.handle.net/11343/274301

Understanding Charge Transfer on the Clinically Used Conical Utah Electrode Array: Charge Storage Capacity, Electrochemical Impedance Spectroscopy and Effective Electrode Area

Alexander R. Harris[1]

[1] Aikenhead Centre for Medical Discovery, ARC Centre of Excellence for Electromaterials Science, Faculty of Medicine, Dentistry and Health Sciences, University of Melbourne, Melbourne, Vic, 3010, Australia

Email: alexrharris@gmail.com

Abstract

Objective: The Utah electrode is used for pre/clinical studies on neural recording and stimulation. Anecdotal and empirical reports on their performance have been made, resulting in variable testing methods. An in depth investigation was performed to understand the electrochemical behaviour and charge transfer mechanisms occurring on these clinically important electrodes. The impact of electrode geometry and material on performance was determined.

Approach: Platinum and iridium electrodes were assessed by cyclic voltammetry and electrochemical impedance spectroscopy. The effective electrode area was measured by reduction of $Ru(NH_3)_6^{3+}$.

Main Results: Pristine Utah electrodes have little to no oxide present and the surface roughness is less than 30 µm. Pristine iridium electrodes pass charge through capacitance and oxide formation. Hydride and anion adsorption occurs on the platinum electrode. Anodic current oxidises both metal surfaces, altering the charge transfer mechanisms at the electrode-solution interface. Charge storage capacity depends on measurement technique and electrode structure, this simplified number ignores more detailed information on charge transfer mechanisms that can be obtained from cyclic voltammetry. Electrode oxidation increases pseudocapacitance, reducing impedance. Charge transfer was non-homogeneous, most likely due to the electrode geometry enhancing charge density at the electrode tip and base. Oxidation of the electrode surface enhanced charge transfer inhomogeneity. The effective electrode area could be measured by reduction of $Ru(NH_3)_6^{3+}$ and calculated with a finite cone geometry.

Significance: Increasing electrode pseudocapacitance, demonstrated by metal oxidation, reduces impedance. Increasing electrode capacitance offers a potential route to reducing thermal noise and increasing signal-to-noise ratio of neural recording. The effective electrode area of conical electrodes can be measured. The charge density of the conical electrode was greater than expected on a planar disc electrode, indicating modification of electrode geometry can increase an electrodes safe charge injection capacity. In vivo electrochemical measurements often don't include sufficient details to understand the electrode behaviour. Electrode oxidation most likely accounts for a significant amount of variation in previously published Utah electrode impedance data.

Keywords

Platinum; Utah array; electrochemistry; impedance

1. Introduction

Electrodes have been developed to interface with the nervous system to monitor or control its behaviour. Neurons fire action potentials, resulting in a change in local ion concentration. This leads to a change in the local potential, which can be measured by a nearby recording electrode. Electrical stimulation of neurons is achieved by applying charge pulses from an electrode. This charge induces a rearrangement of ions at the neuronal membrane, inducing an action potential.

The recording of neural behaviour is used to classify cell type and network structure. The output can then be used to control prosthetic devices for people suffering trauma or loss of function from diseases such as motor neurone disease. Changes in neural response can also provide feedback for delivery of drug or electrical therapeutics to control disease symptoms such as epileptic seizures [1].

Stimulation of neural activity is used to provide sensory input, as demonstrated by the cochlear implant and bionic vision devices [2][3]. It can also control disease symptoms such as tremor and rigidity for Parkinson's disease sufferers through deep brain stimulation (DBS) [4]. DBS is also being trialled for treatment of other neurological disorders including OCD and depression [5]. Electrical stimulation has also been applied to the peripheral nervous system, with stimulation of the vagus nerve used to control drug resistant epilepsy [6]. Stimulation of the spinal cord can treat chronic pain while stimulation of other nerve targets can control organ function such as bladder control or diaphragm pacing [7].

Successful neural recording from clinical devices generally requires a high signal-to-noise ratio and a stable response over the lifetime of the recipient, which may be decades. A high bandwidth may also be needed with thousands of electrodes recording the response of large regions of neural tissue. A stimulating electrode also needs to be able to deliver sufficient charge to induce neural activity without corroding or producing cytotoxic species. To achieve this, several electrode designs have been developed. The majority of clinically approved implantable electrodes are platinum or platinum/iridium [7]. DBS electrodes have large geometric surface areas (~0.06 cm^2) [8] as do electrodes for interfacing with the PNS for stimulating the vagus nerve or spinal cord; cochlear implants are smaller (~0.3 mm^2), [9][10] and the thin film Argus II Bionic Vision electrodes are 0.03 mm^2 [3][11]. Penetrating electrodes for interfacing with the cortex or PNS have even smaller dimensions. The Neuronexus research electrode array has planar electrodes along a silicon shank with areas ~400 μm^2 [12]. The only 510k cleared penetrating microelectrode is the Utah array, which has conical shaped electrodes on top of silicon pillars with electrode areas of ~3000 μm^2 (this work).

The Utah array (Figure 1) has been used to record activity from the cortex of patients to control movement of prosthetic limbs [13]. While performance varies across subjects, typically much lower

neural activity is detected on implants that are more than a year old, compared to those only a few months old [14]. Failure mechanisms associated with the Utah array include electrode breakage, cracking or delamination of insulation, electrode corrosion and degradation of electronics or connectors [15][16][17][18]. Variable performance may be due to movement of the electrode or neural rearrangement, protein fouling and foreign body response, and changes to the electrode structure over time or from current passage [19]. The relationship between benchtop and *in vivo* electrochemical response with electrophysiological performance is still debated. Recent electrochemical and electrophysiological studies of planar Michigan style electrodes have demonstrated impedance at low frequencies is dependent on electrode area, providing a better predictor of thermal noise and signal-to-noise ratio of multiunit activity than the typically reported impedance at 1 kHz [20]. The safe charge storage capacity and charge injection capacity of planar electrodes were seen to be highly dependent on conditions [21][22][23]. In order to understand the electrochemical data obtained with the conical Utah array, its relationship to planar style electrodes, and changes in *in vivo* electrochemical and electrophysiological response over time, a greater understanding of the charge transfer mechanisms that occur on the electrode is required. The effect of electrode geometry on electrochemical and electrophysiological response must be understood. This article investigates the charge storage capacity, impedance, effective electrode area and charge density at platinum and iridium oxide Utah arrays. The implications for electrophysiological and clinical applications is then discussed.

2. Experimental Methods

Sodium chloride, potassium chloride, calcium chloride, hexaammineruthenium(III) chloride ($Ru(NH_3)_6Cl_3$) (Sigma-Aldrich), magnesium chloride hexahydrate (Scharlau) and disodium phosphate (Biochemicals) were used as received. An artificial cerebrospinal fluid (aCSF) contained 2.5 mM KCl, 125 mM NaCl, 21.26 mM $CaCl_2$, 1.18 mM $MgCl_2$ and 2 mM Na_2HPO4. Electrodes were platinum (#15295-25, Mar 2017) or iridium oxide (#15271-27, Feb 2017) Utah arrays (ICS-96, Blackrock Microsystems, supplied by Scitech). The iridium oxide (IrOx) electrodes were previously supplied as anodically activated iridium oxide films (AIROF), but are now supplied as sputtered iridium oxide films (SIROF). Five electrodes on one array of each type were tested. The electrodes were not cleaned before use and had not been used for any *in vivo* studies. Electrodes were tested in a 3-electrode configuration using a Ag/AgCl (3 M KCl) as reference electrode and Pt wire as counter electrode. Experiments were performed on a CHI660E potentiostat (CH Instruments). The electrodes were connected to the potentiostat via a headstage and alligator clips and placed into a beaker of solution. Test solutions were degassed with nitrogen for at least 10 minutes before performing electrochemistry. The effective electrode area was measured by the addition of 5 mM $Ru(NH_3)_6Cl_3$ to the test solution. The impact of solution composition and oxygen concentration on electrochemical

response, details on measuring the effective electrode area and their relationship to clinical application are discussed in [21].

Charge storage capacity measurements were performed using cyclic voltammetry over a range of 0.8 to -0.8 V vs Ag/AgCl at a scan rate of 100 mV s^{-1}. Electroactive area measurements were undertaken over a range of 0.2 to -0.5 V varying the scan rate from 5 mV s^{-1} to 6 V s^{-1}. Electrochemical impedance spectroscopy (EIS) was performed at 0 V vs Ag/AgCl with a 10 mV amplitude over a frequency range of 0.1 to 100,000 Hz. Equivalent circuit fitting of the EIS data was performed with ZView.

3. Results

Cyclic Voltammetry of Platinum and Iridium Oxide Utah Electrodes

Cyclic voltammetry was performed for 2 potential cycles on unused electrodes to investigate the charge transfer mechanisms that occur on pristine Utah electrodes. A simple 0.1 M NaCl solution was used initially to assess the reaction mechanisms occurring at the electrode surface. The electrochemical response is similar to previous reports in PBS [24]. A platinum electrode displayed a reduction shoulder at -520 mV and a peak at -681 mV (Figure 1a). Switching the sweep direction, a broad oxidation peak appeared at -505 mV with rises in oxidation current beginning at approximately -172 mV and 330 mV. On the second cycle, a large, broad reduction process started around 100 mV with the reduction peak at -692 mV. The second oxidation sweep was similar to the first sweep.

Cyclic voltammetry of new platinum electrodes in aCSF had slight differences in response to 0.1 M NaCl (Figure 1b). The reduction shoulder on the first cycle occurred around -504 mV and the reduction peak at -691 mV. On the oxidation sweep, the broad peak occurred at -501 mV and further rise in oxidation current beginning near -130 mV. The second reduction sweep showed a broad reduction process starting around 275 mV with a reduction peak at -675 mV. Once again the second oxidation sweep was unchanged from the first.

The first cycle of an IrOx electrode in 0.1 M NaCl showed a reduction current beginning around -310 mV and a large oxidation current starting at 175 mV (Figure 1c). On the second cycle, a large reduction current begun at 290 mV with no change in the other processes. When an IrOx electrode was placed into aCSF, on the first potential cycle a small reduction current begun at -305 mV, an oxidation peak appeared at 208 mV and large oxidation current started at 410 mV (Figure 1d). On the second cycle, a small reduction process occurred at 427 mV with a larger process beginning at 190 mV. The oxidation peak at 211 mV was slightly larger than in the first cycle while the broad oxidation process from 410 mV was unchanged.

The charge storage capacity (CSC) of both electrode types in aCSF was calculated for each reduction or oxidation sweep by integrating the current-time curve (Table 1) [25]. The platinum electrode has a reduction CSC over 4 times greater than the oxidation CSC. Cycling the electrode potential increased the reduction CSC with little impact on the oxidation CSC. The pristine IrOx had similar oxidation and reduction CSC. After a potential cycle, the reduction CSC increased by a third with little change in the oxidation CSC. The reduction CSC of IrOx is 2-3 times greater than platinum while the oxidation CSC was nearly 10 times larger.

Electrochemical Impedance Spectroscopy of Platinum and Iridium Oxide Utah Electrodes

EIS of each electrode was performed in aCSF immediately before and after 2 cyclic voltammograms from 0.8 to -0.8 V at a scan rate of 100 mV s^{-1}. The response is again similar to previous reports in PBS [24][16]. A typical Nyquist plot of a platinum electrode displays a curved response with decreased radius after potential cycling (Figure 2a). The total impedance increases with decreasing frequency, levelling off below 10 Hz (Figure 2c). The total impedance nearly halved after potential cycling (Table 2). The phase angle was around -70 degrees at high frequencies and approached 0 degrees at low frequencies (Figure 2e). The phase angle shifted closer to 0 degrees after potential cycling.

The platinum EIS could be fit with an equivalent circuit comprising resistors (R1 and R2) and a constant phase element (CPE1). R1 models the solution resistance (which is dependent on electrode geometry); the electrode/solution interface is modelled as a parallel constant phase element (CPE1) and polarisation resistance (R2), the constant phase element is used instead of a capacitor due to surface roughness or inhomogeneity in current distribution at the electrode surface. The significance of fitting this equivalent circuit was high, with an average χ^2 over 5 electrodes of 2.1×10^{-3} before, and 9.2×10^{-4} after voltammetry. Values for the fitted resistance, admittance (Y_0) and power (n) terms for the constant phase element are listed in Table 3. There was a slight increase in solution resistance after cyclic voltammetry, while the admittance doubled and the polarisation resistance halved.

The Nyquist plot of IrOx electrodes produced a linear response before voltammetry and had a slight curvature after voltammetry (Figure 2b). The total impedance was nearly constant at high frequencies and began increasing below 10 kHz (Figure 2d). Once again, the total impedance decreased after potential cycling by over 70 % (Table 2). The phase angle was close to -30 degrees at high frequencies and -60 degrees at low frequencies (Figure 2f). After potential cycling the phase angle was closer to 0 degrees at high frequencies and -80 degrees at low frequencies.

Fitting an equivalent circuit to the IrOx electrodes required resistors (R1 and R2), a constant phase element (CPE1) and finite length Warburg diffusion impedance (Wo1). The addition of Wo1

accounts for the Faradaic processes associated with the iridium oxide. The significance of fitting this equivalent circuit was again high, with an average χ^2 over 5 electrodes of 1.2×10^{-3} before, and 1.8×10^{-2} after voltammetry. The fitted parameters, including a diffusion resistance (R_D) and diffusional time constant (τ_D) associated with the Warburg impedance are listed in Table 3. Similar to the platinum electrodes, after cyclic voltammetry, there was a slight increase in solution resistance. The admittance increased 5 fold, polarisation resistance was 10 times smaller, the diffusion resistance decreased 5 fold and the diffusional time constant was slightly smaller.

Effective Electrode Area of Platinum and Iridium Oxide Utah Electrodes

The effective electrode area of the electrodes was measured by the addition of $Ru(NH_3)_6^{3+}$, which undergoes a one electron reduction

$$Ru\left(NH_3\right)_6^{3+} + e^- \rightleftharpoons Ru\left(NH_3\right)_6^{2+}$$

At fast scan rates, a peak shaped voltammetric response is seen with a peak current according to

$$i_p = (2.69\times10^5)n^{3/2}AD^{1/2}C\upsilon^{1/2} \quad (1)$$

where n is the number of electrons transferred, D is the diffusion coefficient (9.0×10^{-6} cm^2 s^{-1}) [26], C is the concentration and ν is the scan rate. At fast scan rates (short measurement times), a linear diffusion profile of $Ru(NH_3)_6^{3+}$ towards the electrode surface occurs and it is reduced at regions of the electrode that are electrochemically active.

The $Ru(NH_3)_6^{3+}$ process was clearly visible on platinum electrodes, but there was some overlap with background electrochemistry on the IrOx (Figure 3a and b). On platinum at a scan rate of 2 V s^{-1}, a reduction peak at -201 mV and oxidation peak at -98 mV gives a peak splitting of 103 mV and mid-point potential ($E^{1/2}$) of 150 mV. A linear response of i_p versus $\nu^{1/2}$ was observed at scan rates between 1 to 2.5 V s^{-1}, indicating a linear diffusion profile was occurring. At a scan rate of 2 V s^{-1} on IrOx, the reduction peak was not fully resolved, however the oxidation peak was, with a peak at -111 mV. Calculation of a linear diffusion electroactive area could then be obtained via equation 1 for the reduction peak of the platinum electrode and oxidation peak of the IrOx, and were equivalent within error (Table 4). The diffusion layer thickness (δ) is a function of time (t) with $\delta = \sqrt{2Dt}$. In voltammetry, t is estimated as $1/\nu$, so at a scan rate of 2 V s^{-1} the diffusion length of $Ru(NH_3)_6^{3+}$ is approximately 30 μm. Electrode roughness smaller than this diffusion length would not be detected as an increased electrode area.

At small electrodes or long measurement times, a sigmoidal shaped voltammetric response is obtained. On platinum and IrOx electrodes, a background subtraction of a cyclic voltammogram without the presence of $Ru(NH_3)_6^{3+}$ produced a sigmoidal shaped response (Figure 3c and d). The

steady-state current was independent of scan rate below 5 mV s^{-1}. The steady-state current (i_{ss}) at a disc electrode has the form

$$i_{\text{disc}}^{\text{ss}} = 4nFDCr \quad (2)$$

where F is the Faraday constant and r is the electrode radius [27]. The equivalent disc effective electrode area was significantly greater than the linear diffusion area, and IrOx appeared larger than platinum (Table 4).

The Utah electrode can be more accurately modelled as a finite cone than as a disc (Figure 1c). For a finite cone electrode resting on an infinitely wide insulating substrate, the equation governing the steady-state current is modified to

$$i_{\text{cone}}^{\text{ss}} = 4nFDCr(1+qH^{p}) \quad (3)$$

where the radius is taken from the base of the cone and H is the aspect ratio ($H = h/r$, h being the cone height) [28]. The nominal cone height of the Utah electrode is 50 µm while the radius is 18 ± 12 µm ([24] and http://blackrockmicro.com/electrode-types/), giving a nominal surface area of 3041 μm^2 and an H of 2.78. For H between the values of 0 and 3, q and p are fit analytically as 0.30661, and 1.14466 respectively. The cone electrode of the Utah array sits on top of an insulating pillar with a radius (r_s), not on an infinitely wide insulating substrate. Diffusion of species from below the electrode can therefore occur, increasing the steady-state current. The effect of insulating substrate radius on steady-state current is accounted for by normalising the current

$$I_{\text{cone}}^{\text{ss}} = i_{\text{cone}}^{\text{ss}} / i_{disc}^{\text{ss}} = A + B(RG - C)^{D} \quad (4)$$

where $RG = r_s/r$, and A, B, C and D depend on the H value, at an $H = 3$, they are 2.0585, 0.8910, -0.1900 and -1.0288 respectively [28] . A finite cone on a wide insulating substrate has an RG of over 100 while the Utah array has an RG of ~1. $I_{\text{cone}}^{\text{ss}}$ on the Utah electrode is therefore 2.8 (the steady-state current at the conical electrode is 2.8 times greater than a disc electrode of the same radius). And the steady-state current of the Utah array is ~1.36 times higher than that determined from equation 3 where the cone electrode would be mounted on an insulating substrate. Therefore, assuming a cone height of 50 µm and an RG of 1, the basal radius and the effective surface area of the Utah electrode can be calculated and indicate both electrode materials have similar and slightly smaller areas than the nominal values (Table 4).

Charge Density of Platinum and Iridium Oxide Utah Electrodes

The charge density of an electrode is obtained by dividing the CSC by the electrode area. The CSC of platinum and IrOx varies with experimental conditions, including potential sweep direction and potential cycle, resulting in a range of values (Table 1). The electrode area can also be measured by a variety of methods, including a geometric area, or one of the electroactive areas (Table 4). The

charge density of the Utah array was calculated using the CSC from the second cycle of each electrode in aCSF. Two measures of effective electrode area were used; the linear diffusion profile of $Ru(NH_3)_6^{3+}$ at fast voltammetric scan rates; and the steady-state response at slow voltammetric scan rates fit to a finite conical geometry sitting on a pillar. This provides a range of charge density values for platinum and IrOx Utah electrodes (Table 5). The choice of effective electrode area measurement had little impact on the charge density values. IrOx had a 3-fold excess in cathodic charge density and 10 times greater anodic charge density than platinum. Both electrode materials had larger cathodic than anodic charge densities.

4. Discussion

Cyclic Voltammetry, Reaction Mechanisms and Charge Storage Capacity

Neurons communicate via electrochemical signals, enabling their interrogation and control via nearby electrodes. These electrodes are not passive; they are part of an electrical circuit carrying a current. The current is carried by electrons in the electronics and by movement of ions in tissue. The transfer of charge across the electrode-tissue interface can be achieved by rearrangement of ions (capacitance), reduction or oxidation of soluble electroactive species (Faradaic reactions) or reduction or oxidation of the electrode surface (pseudocapacitance). Charge transfer at an ideally polarisable interface would only pass current through capacitance, while an ideally non-polarisable interface would only pass current through Faradaic reactions. In reality, no electrode is ideal, and charge transfer at the electrode-tissue interface is achieved through a mixture of reaction mechanisms [29].

The performance of an electrode in interacting with neurons depends on the reaction mechanisms that occur at the electrode-tissue interface. This includes the signal-to-noise ratio of electrophysiological recordings, the electrode stability in the corrosive tissue environment and during current passage, and the cytocompatibility of any electrochemically generated species [7]. Electroanalytical measurements are made on implantable electrodes to understand the reaction mechanisms that may occur during their clinical use. It may then allow development of new electrode materials, geometries or stimulation waveforms to improve their clinical performance.

Platinum and IrOx electrodes can support numerous electrochemical reactions. However, the reactions which occur are highly dependent on the conditions at the electrode surface. The electrode-tissue structure and composition, reaction thermodynamics and kinetics will determine which reactions actually occur. To understand these reaction mechanisms, cyclic voltammetry is often used. Cyclic voltammetry involves measuring the current passing through an electrode surface while sweeping the potential at a controlled rate. The technique enables the measurement of the thermodynamics and kinetics of electrochemical reactions. Careful control of experimental conditions also allows investigation of the reaction mechanisms occurring.

The platinum Utah array is a sputtered metal film on a conductive silicon substrate [30]. The first voltammetric cycle of a pristine platinum electrode in a simple degassed 0.1 M NaCl solution displays no reduction current associated with platinum oxide reduction and very large, symmetrical peaks typical of a surface confined reaction in the hydrogen adsorption region (Figure 1a). The position and number of peaks in the hydrogen adsorption region provides information on the crystal structure of a platinum electrode [31]. The voltammetry indicates the pristine electrodes have little-to-no platinum oxide present and the crystal structure of the platinum is quite uniform. On the first oxidation sweep, hydrogen desorption occurs and there is an oxidation current indicating formation of platinum oxide. On the second reduction sweep, there is a clear change in the voltammetric response due to the reduction of platinum oxide formed during the first voltammetric cycle. The formation of this oxide layer has also disrupted the pristine platinum surface, decreasing the current associated with hydrogen adsorption.

A pristine platinum electrode placed into aCSF displays very similar voltammetry to 0.1 M NaCl (Figure 1b). There is little platinum oxide present initially, and a large hydrogen adsorption process is visible. On the oxidation sweep, hydrogen desorption occurs, but there is a change in shape in the platinum oxide formation region. This change is consistent with phosphate anion adsorption on the platinum surface, which is not seen in the simpler electrolyte [21].

The IrOx Utah array was previously supplied as sputtered metal which was anodically oxidised, it is now supplied as sputtered iridium oxide and is not electrochemically activated [16]. The first reduction sweep of a pristine electrode in 0.1 M NaCl is almost featureless, the small reduction current beginning at -310 mV is most likely reduction of residual oxygen present in solution (Figure 1c). The large oxidation current on the reverse sweep is due to the formation of iridium oxide. The second reduction sweep shows a new reduction process consistent with reduction of the just formed iridium oxide. The oxidation sweep of a pristine IrOx electrode in aCSF was slightly different in shape, suggesting phosphate anion adsorption also affects the iridium oxide formation (Figure 1d). These voltammetric responses indicate the pristine IrOx Utah electrodes have no electrochemical evidence of oxide present when received they are iridium metal, the iridium oxide forms when an anodic current is applied.

Typically the cathodic CSC of implantable electrodes is reported. A larger CSC measured by cyclic voltammetry generally results in a smaller change in potential when a current pulse is applied to the electrode [22]. On an ideally polarisable electrode, with charge only supplied by capacitance across the electrode-tissue interface, the anodic and cathodic CSC would be identical. Platinum and IrOx are not ideal electrodes, so the anodic and cathodic CSC are different (Table 1). The CSC of each

electrode depends on what reactions occur on each potential sweep. In saline solutions, pristine platinum electrodes mainly transfer charge through capacitance and hydrogen adsorption/desorption while pristine iridium electrodes mainly pass capacitance. Both electrode materials undergo changes when an anodic current is passed through them, with the formation of metal oxides. These used electrodes may display similar CSC values to pristine electrodes, but the charge transfer mechanisms have changed with less hydrogen adsorption/desorption occurring and greater charge associated with oxide formation and removal. Changes to the solution composition will also affect the reaction mechanisms occurring, such as anion adsorption [21].

The typically reported CSC is measured between the water oxidation and reduction potentials (water window) assuming only the reactions occurring outside this potential range are damaging to the electrode and nearby tissue. However platinum and iridium oxide formation and removal clearly occurs within the water window. These reactions are associated with electrode corrosion and the formation of cytotoxic species. On DBS and cochlear implants, the electrodes are either encapsulated in glial tissue or surrounded by perilymph, so the electrode is not in intimate contact with the target neural tissue. Corrosion may occur, damaging the electrode, but formation of cytotoxic species may have limited impact on the target neural tissue [32]. For cortical implants such as the Utah array, the electrode is in close contact with the target neural tissue. Encapsulation of the electrode by glial tissue leads to a decrease in performance, and electrode corrosion exposes the target neural tissue to potentially cytotoxic species [33]. The metal films used for DBS and cochlear implants are also relatively thick, so small amounts of electrode corrosion would have minimal impact on device lifetime. However the Utah array has a thin metal film, so that corrosion may completely remove the functional electrode. As a result, the reporting of a single CSC value for an electrode is too simplistic. The anodic and cathodic CSC are not equivalent, limiting the use of a CSC measured from only one potential sweep. The charge transfer mechanisms that occur on an electrode surface change with conditions and over time, so the choice of testing solution and method can affect the CSC value. And the measurement of CSC within the water window ignores the possibility of other damaging reactions that may occur, such as the reduction of oxygen to oxygen radicals, so that an electrodes safe CSC can be significantly reduced. CSC is also measured from a slow potential sweep cyclic voltammogram, however electrical stimulation of tissue is usually achieved through short current pulses. Charge injection capacity (CIC) measured from chronopotentiometry is more closely related to their clinical use. In general there is good agreement between CSC and CIC values, however shorter current pulses will pass less charge from kinetically slow reactions than slow potential sweeps, the specific reaction mechanisms occurring depend on pulse waveform, and analysing the mechanisms occurring during a chronopotentiometic response is difficult [34][23]. Great care must therefore be taken when assessing the performance of implantable electrodes using CSC and CIC. They can provide a guide to the

amount of charge that an electrode can pass, but more electrochemical mechanistic details are required.

Electrochemical Impedance Spectroscopy and Signal-to-Noise Ratio

The impedance of implantable electrodes is usually reported in the literature. In this technique, a small alternating signal (~5-10 mV amplitude) is applied to the electrode, rather than the large perturbation (1-2 V) used in cyclic voltammetry. The use of a small perturbation ensures the electrochemical system is in a steady-state condition (at equilibrium) and the current-potential relationship can be considered linear, simplifying its analysis. Under linear conditions, an applied alternating potential generates a current of the same alternating behaviour; however, when large perturbations are applied in an electrochemical cell, the current-voltage relationship becomes nonlinear and the current response is distorted. In EIS, the applied perturbation is typically a sinusoidal voltage swept over a range of frequencies. The measured EIS is then fit with an equivalent electrical circuit. Components in the equivalent circuit are then assigned to various aspects of the electrochemical system. EIS can therefore provide information on the kinetics of an electrochemical system.

EIS of the platinum Utah electrodes could be fit with an equivalent circuit producing a single time constant (Figure 2). It comprised a resistance to account for the solution and a parallel constant phase element and resistor to model the electrode-solution interface. The pristine electrode, with minimal platinum oxide present, behaves as an imperfect capacitor. The deviation from a perfect capacitor is due to inhomogeneous current distribution across the electrode surface. As the chemical composition of the electrode surface appears uniform and the surface roughness is low, this deviation is most likely caused by the complex electrode geometry. Previous modelling of charge density at a conical electrode has shown there is a higher charge density at the electrode tip and at the electrode-insulator interface [35]. However this type of modelling assumes uniform composition of the electrode and surrounding tissue and ignores any electrochemical reactions that may occur. In an equivalent circuit with a parallel CPE and resistor, the admittance can be used to calculate a capacitance value

$$C = Y_0(\omega_{\mathrm{m}}^{''})^{\mathrm{n}-1} \tag{5}$$

where $\omega_{\mathrm{m}}^{''}$ is the frequency at which the imaginary impedance (Z'') is a maximum [36].

After voltammetry, the EIS response could be fit with the same equivalent circuit, however the admittance increased and charge transfer resistance decreased (Table 3). The formation of platinum oxide during voltammetry has effectively increased the electrode pseudocapacitance. The power term has also decreased, indicating surface oxidation has reduced the current homogeneity and the platinum oxide layer may not be homogeneous. Longer term stimulation or implantation can lead to

electrode delamination and corrosion, cracking or delamination of insulation and gliosis, further impacting on impedance and current homogeneity [16][18].

EIS of the IrOx Utah array was fit with an equivalent circuit generating 2 time constants. This equivalent circuit models the solution resistance, a parallel constant phase element and resistor modelling the electrode-solution interface, and a Warburg diffusion impedance to account for the iridium oxidation reactions. The behaviour of the pristine IrOx electrode is similar to platinum, but has a higher admittance and lower polarisation resistance. Further oxidation of the iridium, increases the admittance and the polarisation resistance decreases, consistent with previous studies on iridium Neuronexus electrodes [37]. The effective pseudocapacitance of the electrode increasing with iridium oxidation.

Platinum and iridium oxidation was found to increase the electrode's effective pseudocapacitance as measured by EIS and the cathodic CSC, however the anodic CSC was unaffected. An increased electrode capacitance lowers the total electrode impedance ($|Z|$) [23]. Typically the impedance at 1 kHz is used to assess an electrodes performance. The impedance at 1 kHz of both electrode materials decreased after oxidation (Table 2). Measurement of impedance at one frequency provides no information about a systems equivalent circuit or the reaction mechanisms occurring at the electrode-tissue interface. However the single impedance value can be used to predict signal-to-noise ratio of electrophysiological recordings [20]. Thermal noise (V_{rms}^{th}) is generated through a resistor (R)

$$V_{rms}^{th} = \sqrt{4k_b TR\Delta f} \tag{6}$$

where k_b is Boltzmann's constant, T is the absolute temperature and Δf is the measuring bandwidth. In an RC circuit, this is modified to

$$V_{rms}^{th} = \sqrt{\frac{k_b T}{C}} \tag{7}$$

A decrease in electrode resistance or increase in capacitance lowers the thermal noise and increases the recording signal-to-noise ratio. Changes to impedance of the Utah array have been seen by changing electrode material and area [38]. A reduction in thermal noise and increase in signal-to-noise ratio has been achieved through increasing electrode area, which reduces resistance and increases capacitance [20][39]. However this also increases the number of neurons detected by the electrode, reducing the measurement specificity. The increase in pseudocapacitance by oxidation of pristine platinum and iridium should also reduce thermal noise, which would enable an increase in signal-to-noise ratio without affecting detection specificity. Animal studies testing this will be published shortly.

The EIS response of an electrochemical system is a function of the electrical double layer formed at the electrode-tissue interface. In simple systems, the behaviour of the electrical double layer dominates the low frequency response while the bulk electrolyte dominates the high frequency response. The transition frequency in the EIS from one layer to the other is dependent on each layers dielectric constant and conductivity [20]. It is difficult to measure this transition frequency and it will vary in biological systems. The thermal noise is controlled by the electrical double layer, and therefore low frequency impedance is a better predictor of electrode performance. This has been demonstrated with stronger prediction of thermal noise and signal-to-noise ratio using impedance at 12 Hz than the usually reported 1 kHz [20]. The impedance of platinum and IrOx electrodes at 10 Hz is reported here for reference (Table 2).

Effective Electrode Area and Charge Density

The impedance, thermal noise and signal-to-noise ratio of neural recordings are a function of electrode area. The amount of charge that can be safely delivered from an electrode also depends on electrode area. An assessment of the safe charge delivery is calculated by dividing the CSC by electrode area, providing a charge density. The electrode area can be measured by different methods, providing nominal, geometric or effective areas. A nominal area assumes manufacturing processes are perfect and reproducible, which is rarely true. A geometric area can be measured by microscopy. Geometric area measurements are simple for planar 2-dimensional electrodes, but are less accurate for more complex electrode geometries such as the 3-dimensional, conical Utah arrays, or when the electrode has a high surface roughness. A geometric area also assumes the entire electrode is functional, which may not be true after protein or cell adsorption, or electrode corrosion [40]. Electrochemical methods allow the measurement of an effective electrode area, providing rapid measurement of functional electrode area even on complex electrode geometries and with non-uniform functionality.

The effective electrode area was measured at short (radial diffusion dominant) and long (linear diffusion dominant) times using the reduction of $Ru(NH_3)_6^{3+}$. This redox reaction is highly reversible and is an outer sphere reaction (electron transfer occurs without disrupting the $Ru(NH_3)_6^{3+}$ hydration layer), making it suitable for many electrode materials. It has already been applied to platinum, iridium oxide and conducting polymer coated neural electrodes and cochlear implants [21][12][41][42][43]. Measurements made at long time periods can provide effective electrode areas that ignore surface roughness. Short measurement times will provide an effective electrode area that includes surface roughness. The effective electrode area of the Utah array was unaffected by measurement time, indicating the surface was very smooth (less than 30 μm). After long term implantation, corrosion and surface rearrangement can increase the surface roughness [18].

Differences in effective electrode area at short and long time measurements would then be expected, and the surface roughness could be detected electrochemically.

The effective area at a conical electrode at long time periods can be calculated with equations 2-4. In calculating the area, the electrode height, radius and substrate radius must be solved. It was assumed that the substrate radius was equal to the electrode radius. The conical electrodes of the Utah array sit on substrate pillars, which project significantly above the bonding pad. There is a thin layer of dielectric coating on the substrate pillars, which make the substrate radius slightly larger than the electrode radius, but this will have minimal impact on diffusion of $Ru(NH_3)_6^{3+}$ to the electrode surface. The nominal cone height is given as 50 µm while the nominal radius has some error, therefore the electrode height was fixed and the radius varied. It is likely that there is some variation in electrode height and this would also affect the calculated radius, however this would have minimal effect on the values for total area.

The current for reduction of $Ru(NH_3)_6^{3+}$ produced an effective area of a cone geometry that was significantly smaller than for a disc geometry (Table 4). This is due to enhanced diffusion of $Ru(NH_3)_6^{3+}$ to the cone electrode.

The charge density values depend on conditions and measurement technique. The second cycle of a cyclic voltammogram was used to measure CSC, as the pristine electrodes present on the first cycle are not stable and poorly reflect their clinical use. Due to the low surface roughness, either effective electrode area could be used in this study. Previous measures of platinum's charge density on planar electrodes under a wide range of conditions significantly exceeding those encountered *in vivo* was 0.15 to 5.57 mC cm^{-2} [21]. The charge density on the platinum Utah electrodes ranged from 2.3 to 13.0 mC cm^{-2} (Table 5). If the charge density of the Utah array was calculated with the equivalent disc area, then the range would be 1.15 to 6.5 mC cm^{-2}, a very similar range to previous reports. Clearly the 3-dimensional geometry of the electrode has increased the charge density. This raises the possibility of optimising electrode geometry to increase their safe charge density.

The charge density of IrOx can vary significantly with conditions, in particular the amount of oxide present. Previous reports of charge density of anodically formed IrOx on Neuronexus electrodes using an effective electrode area ranged from 9.7 to 529.5 mC cm^{-2} [43]. The charge density of the Utah array with a very thin layer of oxide ranged from 22.0 to 34.1 mC cm^{-2}. Further increases in charge density could be achieved by increasing the thickness of oxide [43]. This range will also be enhanced by the electrode geometry, compared to planar electrodes.

Implications for in vivo performance

Electrochemical studies on the Utah array have been performed in vivo, but inconsistencies and limitations in their measurement and reporting are common, reducing their utility. An early report implanted the Utah array in a feline cortex over a year [44]. Histology indicated fibrous tissue encapsulation around most implants. A 10 nA sinusoidal current was applied at 1 kHz to assess the electrode impedance. The measured response was variable or decreased slightly over time and it was speculated that changes to the insulation were the cause.

A study of SIROF Utah arrays was also implanted in feline cortex for nearly a year [45]. Small changes in anodic and cathodic CSC were seen from before implantation in artificial interstitial fluid and over time in vivo depending on the voltametric scan rate. The impedance was measured with a 10 mV sinusoidal voltage and indicated an increase in high frequency impedance when comparing in vitro to in vivo response, but there appeared to be minimal change at low frequencies. It was speculated that the impedance changes were caused by biofouling processes and the changes seen in CSC were due to cracking of the insulation.

The IrOx and platinum Utah array were compared against other electrode geometries in a rat cortex for a month [46]. It is unclear what potential range was used to determine the CSC. The impedance was measured at 1 kHz and was extremely variable over the study. The impedance and CSC were then averaged across the entire array, preventing any detailed analysis of electrode performance.

Utah arrays have been implanted into the cortex of Rhesus macaques for 6 months and subject to a charge balanced biphasic stimulation protocol [19]. The electrodes were iridium coated with SIROF. The impedance was measured with a 10 nA sinusoidal current at 1 kHz. The impedance value decreased with electrical stimulation, and decreased at a faster rate when larger or longer charge pulses were applied. The authors suggested the changes in impedance could be caused by movement of encapsulating tissue, electrode oxidation, insulation failure or electrode failure, but no data was available to support these mechanisms.

From these in vivo studies, it is unclear what condition the electrodes were in before implantation. The measurements performed also prevent any real understanding of the electrode behaviour when implanted. Gross changes in electrochemical behaviour as tested by impedance measurements at 1 kHz or a single cyclic voltammogram can indicate electrode failure due to lead breakage or shorting but provide no details on the charge transfer mechanisms or structure of the electrode tissue interface. In general, the data reported from these in vivo studies are in agreement with the in vitro measurements detailed in this article. Unless electrodes are deliberately activated or modified before use, they have no electrochemical evidence of metal oxide. Application of an anodic current oxidises the metal electrode surface, reducing its impedance and increasing its CSC. The increase in electrode

pseuodocapacitance should lead to a reduction in thermal noise and increase in signal-to-noise ratio compared to the pristine metal. However biological noise (variation in the number of neurons near the electrode and the electrode-neuron distance) can have an order of magnitude effect on signal-to-noise ratio, and likely plays a bigger role in variable electrophysiological performance [25]. Care must be taken when assessing changes to the CSC, the oxidation of metal electrodes may lead to corrosion and formation of cytotoxic species [7]. Simplifying cyclic voltammetry to a single CSC value ignores the electrochemical mechanisms occurring at the electrode-tissue interface and how they change over time. Further studies on the effect of biofouling on electrochemical behaviour of implantable electrodes will be published shortly.

5. Conclusions

The electrochemical performance of platinum and IrOx Utah arrays was assessed. The pristine electrodes had little to no oxide present and the surface roughness was less than 30 µm. Charge transfer at the electrode surface is non-ideal. A pristine iridium electrode passes charge through capacitance and oxide formation. Hydride adsorption occurs on the platinum electrode, and anion adsorption is also possible. Application of an anodic current oxidises both metal surfaces, changing the charge transfer mechanisms at the electrode-solution interface. The CSC depends on measurement technique and electrode structure, providing no information on the charge transfer mechanisms occurring during a cyclic voltammogram. Electrode oxidation increases its pseudocapacitance, which reduces its impedance. This should reduce the thermal noise and increase its signal-to-noise ratio when recording neural activity. Fitting the impedance response on the conical Utah electrodes required a constant phase element, indicating non-homogeneous charge transfer. This is most likely due to the geometry of the electrode enhancing charge density at the electrode tip and base. Oxidation of the electrode surface enhanced the inhomogeneity of charge transfer. The effective electrode area could be measured by the reduction of $Ru(NH_3)_6^{3+}$ and calculated from a finite cone geometry. The charge density of the conical electrode was greater than expected on a planar disc electrode, indicating modification of electrode geometry can increase an electrodes safe charge injection capacity.

Acknowledgements

Funding from the Australian Research Council Centre of Excellence Scheme (Project Number CE140100012) is gratefully acknowledged.

References

[1] Cook M J, O'Brien T J, Berkovic S F, Murphy M, Morokoff A, Fabinyi G, D'Souza W, Yerra R, Archer J, Litewka L, Hosking S, Lightfoot P, Ruedebusch V, Sheffield W D, Snyder D, Leyde K and Himes D 2013 Prediction of seizure likelihood with a long-term, implanted

seizure advisory system in patients with drug-resistant epilepsy: a first-in-man study *Lancet Neurol.* **12** 563–571

[2] Clark G 2009 The multi-channel cochlear implant: Past, present and future perspectives *Cochlear Implants Int.* **10** 2–13

[3] Stronks H C and Dagnelie G 2014 The functional performance of the Argus II retinal prosthesis *Expert Rev. Med. Devices* **11** 23–30

[4] Lukins T R, Tisch S and Jonker B 2014 The latest evidence on target selection in deep brain stimulation for Parkinson's disease *J. Clin. Neurosci.* **21** 22–7

[5] Kennedy S H, Giacobbe P, Rizvi S J, Placenza F M, Nishikawa Y, Mayberg H S and Lozano A M 2011 Deep Brain Stimulation for Treatment-Resistant Depression: Follow-Up After 3 to 6 Years *Am. J. Psychiatry* **168** 502–10

[6] Ohemeng K K and Parham K 2020 Vagal Nerve Stimulation: Indications, Implantation, and Outcomes *Otolaryngol. Clin. North Am.* **53** 127–43

[7] Harris A R 2020 Current perspectives on the safe electrical stimulation of peripheral nerves with platinum electrodes *Bioelectron. Med.* **3**

[8] Cogan S F 2008 Neural Stimulation and Recording Electrodes *Annu. Rev. Biomed. Eng.* **10** 275–309

[9] Seligman P 2009 Prototype to product—developing a commercially viable neural prosthesis *J. Neural Eng.* **6** 65006

[10] Dhanasingh A and Jolly C 2017 An overview of cochlear implant electrode array designs *Hear. Res.* **356** 93–103

[11] Weiland J D and Humayun M S 2014 Retinal prosthesis *IEEE Trans. Biomed. Eng.* **61** 1412–24

[12] Harris A R, Molino P J, Kapsa R M I, Clark G M, Paolini A G and Wallace G G 2014 Optical and Electrochemical Methods for Determining the Effective Area and Charge Density of Conducting Polymer Modified Electrodes for Neural Stimulation *Anal. Chem.* **87** 738–46

[13] Normann R A and Fernandez E 2016 Clinical applications of penetrating neural interfaces and Utah Electrode Array technologies *J. Neural Eng.* **13** 61003

[14] Downey J E, Schwed N, Chase S M, Schwartz A B and Collinger J L 2018 Intracortical recording stability in human brain–computer interface users *J. Neural Eng.* **15** 46016

[15] Caldwell R, Street M G, Sharma R, Takmakov P, Baker B and Rieth L 2020 Characterization of Parylene-C degradation mechanisms: In vitro reactive accelerated aging model compared to multiyear in vivo implantation *Biomaterials* **232** 119731

[16] Negi S, Bhandari R, Rieth L, Van Wagenen R and Solzbacher F 2010 Neural electrode degradation from continuous electrical stimulation: Comparison of sputtered and activated iridium oxide *J. Neurosci. Methods* **186** 8–17

[17] Nolta N F, Christensen M B, Crane P D, Skousen J L and Tresco P A 2015 BBB leakage,

astrogliosis, and tissue loss correlate with silicon microelectrode array recording performance *Biomaterials* **53** 753–62

[18] Barrese J C, Aceros J and Donoghue J P 2016 Scanning electron microscopy of chronically implanted intracortical microelectrode arrays in non-human primates *J. Neural Eng.* **13** 26003

[19] Chen K H, Dammann J F, Boback J L, Tenore F V, Otto K J, Gaunt R A and Bensmaia S J 2014 The effect of chronic intracortical microstimulation on the electrode–tissue interface *J. Neural Eng.* **11** 26004

[20] Harris A R, Allitt B and Paolini A 2019 Predicting Neural Recording Performance of Implantable Electrodes *Analyst* **144** 2973–83

[21] Harris A R, Newbold C, Carter P, Cowan R and Wallace G G 2018 Measuring the Effective Area and Charge Density of Platinum Electrodes for Bionic Devices *J. Neural Eng.* **15** 46015

[22] Harris A R, Newbold C, Carter P, Cowan R and Wallace G G 2018 Charge Injection from Chronoamperometry of Platinum Electrodes for Bionic Devices *J. Electrochem. Soc.* **165** G3033–41

[23] Harris A R, Newbold C, Cowan R and Wallace G G 2019 Insights into the Electron Transfer Kinetics, Capacitance and Resistance Effects of Implantable Electrodes Using Fourier Transform AC Voltammetry on Platinum *J. Electrochem. Soc.* **166** G131–40

[24] Negi S, Bhandari R, Rieth L and Solzbacher F 2010 In vitro comparison of sputtered iridium oxide and platinum-coated neural implantable microelectrode arrays *Biomed. Mater.* **5** 15007

[25] Harris A R, Morgan S J, Wallace G G and Paolini A G 2014 A Method for Systematic Electrochemical and Electrophysiological Evaluation of Neural Recording Electrodes *J. Vis. Exp.* e51084

[26] Barsan M M, Pinto E M, Florescu M and Brett C M A 2009 Development and characterization of a new conducting carbon composite electrode *Anal. Chim. Acta* **635** 71–8

[27] Bard A J and Faulkner L R 2001 *Electrochemical Methods* (New York: Wiley)

[28] Zoski C G and Mirkin M V 2002 Steady-State Limiting Currents at Finite Conical Microelectrodes *Anal. Chem.* **74** 1986–92

[29] Harris A R and Wallace G G 2019 Electrochemical Methods for Analysing and Controlling Charge Transfer at the Electrode-Tissue Interface *Curr. Opin. Electrochem.* **16** 143–8

[30] Campbell P K, Jones K E, Huber R J, Horch K W and Normann R A 1991 A silicon-based, three-dimensional neural interface: manufacturing processes for an intracortical electrode array *Biomed. Eng. IEEE Trans.* **38** 758–68

[31] Ross Jr P N 1981 Hydrogen chemisorption on Pt single crystal surfaces in acidic solutions *Surf. Sci.* **102** 463–85

[32] Shepherd R K, Carter P M, Enke Y L, Wise A K and Fallon J B 2019 Chronic intracochlear electrical stimulation at high charge densities results in platinum dissolution but not neural loss or functional changes in vivo *J. Neural Eng.* **16** 26009

[33] Bensmaia S J and Miller L E 2014 Restoring sensorimotor function through intracortical interfaces: progress and looming challenges *Nat Rev Neurosci* **15** 313–25

[34] Harris A R, Newbold C, Carter P, Cowan R and Wallace G G 2019 Using Chronopotentiometry to Better Characterize the Charge Injection Mechanisms of Platinum Electrodes Used in Bionic Devices *Front. Neurosci.* **13** 380

[35] McIntyre C and Grill W 2001 Finite Element Analysis of the Current-Density and Electric Field Generated by Metal Microelectrodes *Ann. Biomed. Eng.* **29** 227–35

[36] Hsu C H and Mansfeld F 2001 Technical Note: Concerning the Conversion of the Constant Phase Element Parameter Y0 into a Capacitance *Corrosion* **57** 2

[37] Harris A R and Paolini A G 2017 Correlation of Impedance and Effective Electrode Area of Iridium Oxide Neural Electrodes *Aust. J. Chem.* **70**

[38] Caldwell R, Sharma R, Takmakov P, Street M G, Solzbacher F, Tathireddy P and Rieth L 2018 Neural electrode resilience against dielectric damage may be improved by use of highly doped silicon as a conductive material *J. Neurosci. Methods* **293** 210–25

[39] Harris A R, Morgan S J, Chen J, Kapsa R M I, Wallace G G and Paolini A G 2013 Conducting polymer coated neural recording electrodes *J. Neural Eng.* **10** 016004

[40] Newbold C and et al. 2010 Changes in biphasic electrode impedance with protein adsorption and cell growth *J. Neural Eng.* **7** 56011

[41] Harris A R, Molino P J, Kapsa R M I, Clark G M, Paolini A G and Wallace G G 2016 Effective area and charge density of dextran sulphate doped PEDOT modified electrodes *Synth. Met.* **220**

[42] Harris A R, Molino P J, Paolini A G and Wallace G G 2016 Effective Area and Charge Density of Chondroitin Sulphate Doped PEDOT Modified Electrodes *Electrochim. Acta* **197**

[43] Harris A R, Paolini A G and Wallace G G 2017 Effective Area and Charge Density of Iridium Oxide Neural Electrodes *Electrochim. Acta* **230** 285–92

[44] Rousche P J and Normann R A 1998 Chronic recording capability of the Utah Intracortical Electrode Array in cat sensory cortex *J. Neurosci. Methods* **82** 1–15

[45] Kane S R, Cogan S F, Ehrlich J, Plante T D, McCreery D B and Troyk P R 2013 Electrical Performance of Penetrating Microelectrodes Chronically Implanted in Cat Cortex *Biomed. Eng. IEEE Trans.* **60** 2153–60

[46] Ward M P, Rajdev P, Ellison C and Irazoqui P P 2009 Toward a comparison of microelectrodes for acute and chronic recordings *Brain Res.* **1282** 183–200

Table 1. Charge storage capacity of platinum and iridium oxide Utah electrodes measured from cyclic voltammetry in aCSF over a potential range of 0.8 to -0.8 V at a scan rate of 100 mV s^{-1}.

Electrode	Charge Storage Capacity /nC *			
	Reduction		Oxidation	
	First Cycle	Second Cycle	First Cycle	Second Cycle
Platinum	278 (81)	297 (91)	64 (20)	65 (24)
Iridium Oxide	625 (179)	815 (212)	611 (162)	615 (166)

*Average (standard deviation) of 5 electrodes.

Table 2. Impedance of platinum and iridium oxide Utah electrodes measured before and after 2 voltammetric cycles in aCSF over a potential range of 0.8 to -0.8 V at a scan rate of 100 mV s^{-1}.

Electrode	Impedance / kOhm *			
	1 kHz before voltammetry	10 Hz before voltammetry	1 kHz after voltammetry	10 Hz after voltammetry
Platinum	277 (75)	10000 (2490)	154 (37)	5070 (1180)
Iridium Oxide	46 (24)	964 (562)	13 (5)	227 (60)

*Average (standard deviation) of 5 electrodes.

Table 3. Electrochemical impedance parameters from equivalent circuit fitting measured before and after 2 voltammetric cycles in aCSF over a potential range of 0.8 to -0.8 V at a scan rate of 100 mV s^{-1}.*

Electrode	R_1 /Ω	Q_0 / 10^{-9} S $s^{1/2}$	n	R_2/MΩ	R_D/MΩ	τ_D /ms
Platinum	2640 (160)	2.76 (0.61)	0.83 (0.01)	30.8 (12.7)	-	-
Platinum after CV	3730 (490)	6.20 (1.49)	0.80 (0.02)	16.1 (10.1)	-	-
Iridium Oxide	3430 (600)	74.9 (37.5)	0.68 (0.04)	5.0 (3.3)	134 (277)	5.77 (3.75)
Iridium Oxide after CV	4570 (500)	393 (161)	0.64 (0.08)	0.5 (1.0)	27.7 (31.0)	3.61 (2.69)

*Average (standard deviation) of 5 electrodes.

Table 4. Effective electrode area of platinum and iridium oxide Utah electrodes measured at fast and slow voltammetric scan rates.*

Electrode	Linear diffusion (μm²) §	Radial Diffusion		
		Equivalent Disc (μm²)	Cone +	
			Basal Radius (μm)	Surface Area (μm²)
Platinum	2790 (922)	4490 (1660)	14 (3)	2250 (456)
Iridium Oxide	2410 (579)	6480 (1890)	17 (3)	2760 (459)

*Average (standard deviation) of 5 electrodes. § Reduction sweep used for platinum, oxidation sweep used for iridium oxide. +Assuming a cone height of 50 μm and RG of 1.

Table 5. Charge density of platinum and iridium oxide Utah electrodes measured from the second potential voltammetric cycle in aCSF over a potential range of 0.8 to -0.8 V at a scan rate of 100 mV s^{-1} and effective electrode area measured at fast and slow voltammetric scan rates.

Electrode	Charge Density (mC/cm^2) *			
	Reduction		Oxidation	
	Linear diffusion	Radial diffusion	Linear diffusion	Radial diffusion
Platinum	10.7 (1.0)	13.0 (1.6)	2.3 (0.2)	2.8 (0.5)
Iridium Oxide	34.1 (4.4)	29.3 (4.4)	25.6 (3.0)	22.0 (3.3)

*Average (standard deviation) of 5 electrodes.

Figure Captions

Figure 1. (a-b) 100 electrode Utah array reproduced with permission from [13]. (c) Geometry of the finite conical electrode with metallized tip (height = $\underline{h}$, radius = r) on a parylene coated substrate pillar (radius = r_s) which is attached to the bonding pad.

Figure 2. First two voltammetric cycles of a Utah electrode from 0.8 to -0.8 V at a scan rate of 100 mV s^{-1} (a-b) platinum (c-d) iridium oxide in degassed (a and c) 0.1 M NaCl and (b and d) aCSF.

Figure 3. Electrochemical impedance of a Utah electrode in degassed aCSF at 0 V with an ac amplitude of 10 mV before and after 2 voltammetric cycles from 0.8 to -0.8 V at a scan rate of 100 mV s^{-1}. (a, c, e) platinum (b, d, f) iridium oxide. Equivalent circuits used to model each electrode are shown.

Figure 4. Cyclic voltammetry of a Utah electrode from 0.2 to -0.5 V in degassed 0.1 M NaCl with 5 mM $Ru(NH_3)_6^{3+}$ (a-b) 2 V s^{-1} (c-d) 5 mV s^{-1} with background subtraction, (a and c) platinum, (b and d) iridium oxide electrode.

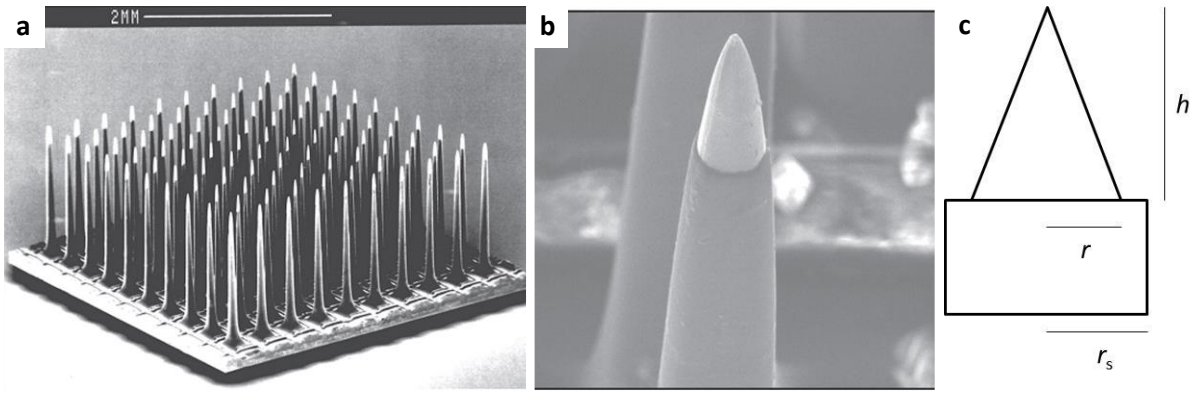


Figure 1

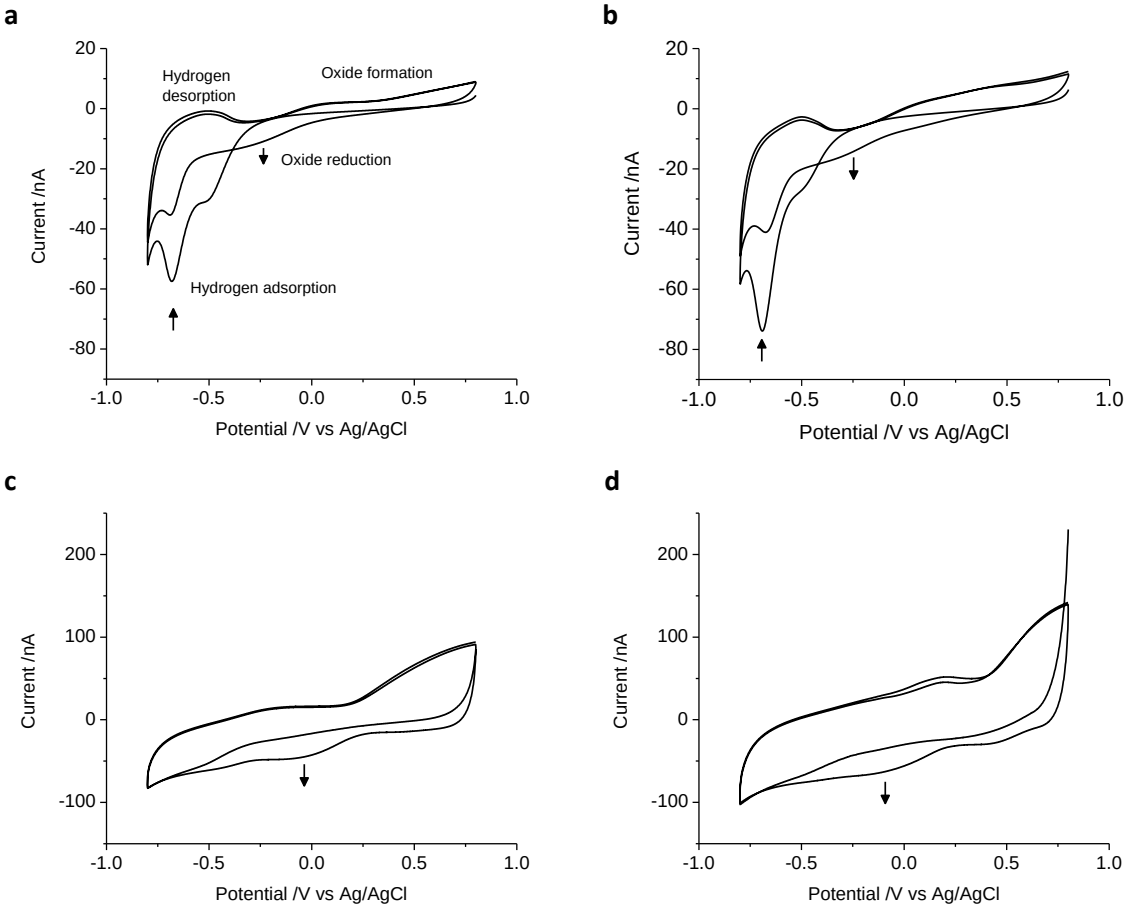

a
b
c
d
Hydrogen desorption
Oxide formation
Oxide reduction
Hydrogen adsorption
Current /nA
Potential /V vs Ag/AgCl

Figure 2

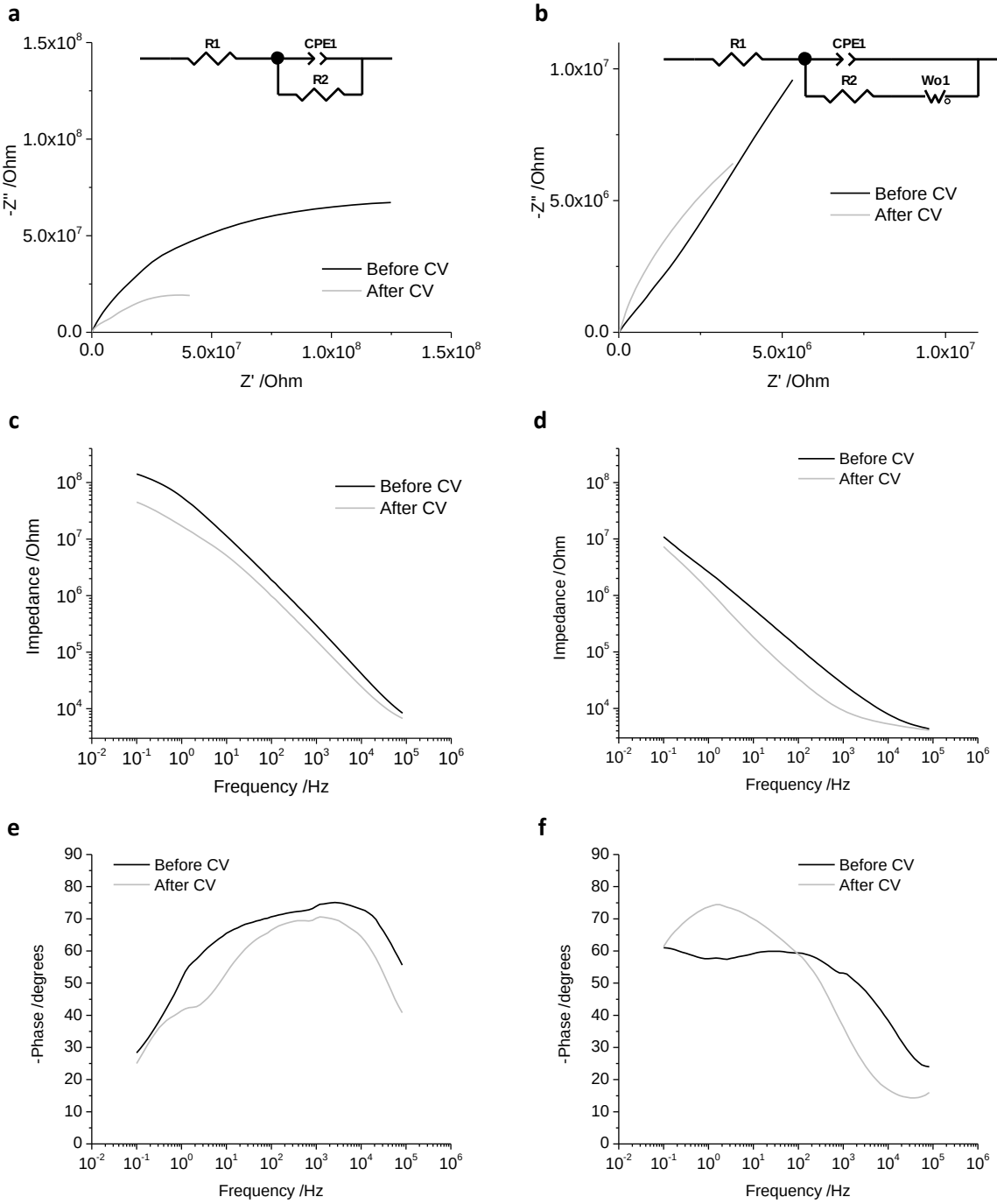

a
R1
CPE1
R2
-Z'' /Ohm
Z' /Ohm
Before CV
After CV
b
R1
CPE1
R2
Wo1
-Z'' /Ohm
Z' /Ohm
Before CV
After CV
c
Impedance /Ohm
Frequency /Hz
Before CV
After CV
d
Impedance /Ohm
Frequency /Hz
Before CV
After CV
e
-Phase /degrees
Frequency /Hz
Before CV
After CV
f
-Phase /degrees
Frequency /Hz
Before CV
After CV

Figure 3

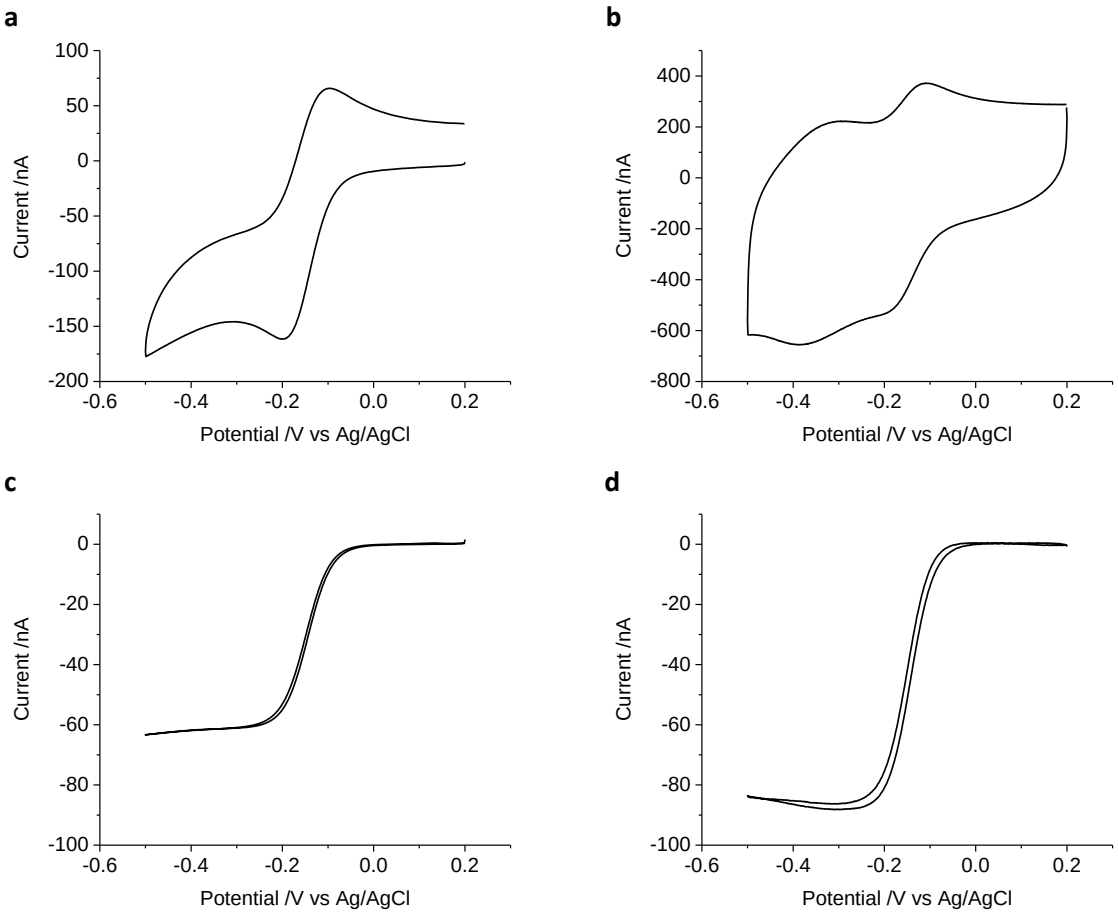

a
b
c
d
Current /nA
Potential /V vs Ag/AgCl
100
50
0
-50
-100
-150
-200
400
200
-200
-400
-600
-800
-20
-40
-60
-80
-0.6
-0.4
-0.2
0.0
0.2

Figure 4